

Measurement of the Inclusive $b\bar{b}$ Jet Production Cross Section

Anant Gajjar, Ronan McNulty, Andrew Mehta, Tara Shears

University of Liverpool

Abstract

We present preliminary measurements of the inclusive $b\bar{b}$ jet production cross section using data taken by the CDF experiment at centre-of-mass energies of 1.96TeV. Two secondary vertex tagged jets within $|\eta| < 1.2$ are required; one of these tagged jets has to have a corrected transverse energy greater than 30GeV, the other has to have a corrected transverse energy greater than 20GeV. We compare our results to Leading Order (Pythia and Herwig) and Next to Leading Order (MC@NLO) predictions.

1 Introduction

There exists a discrepancy between the theoretical prediction and the run I measurement for the inclusive b production cross section made by both CDF [1] and D0 [2]. The measured rate is almost twice as high as that predicted by NLO QCD, this excess could be due to new physics or simply because we do not understand the various production mechanisms in NLO QCD, these mechanisms are discussed in section 2. A recalculation by Cacciari and Nason [3] has shown a reduction in this excess. They also recommend that hadron level cross sections should be presented rather than deconvoluting the results to the quark level.

In this note we briefly explain the analysis procedure: the data and Monte Carlo datasets used for the analysis are described in section 3; section 4 describes the jet energy corrections that have been used, including a b flavour specific correction; event selection and acceptance calculations are described in sections 5 and 6, respectively; the secondary vertex tagging efficiency calculation is discussed in section 7; results are given in section 8; and we conclude in section 9.

2 Production Mechanisms

The leading order and next to leading order production mechanisms can be categorised into three classes, flavour creation, flavour excitation and gluon splitting, figure 1 shows Feynman diagrams for each class. In the flavour creation category the $b\bar{b}$ pair are produced via gluon-gluon fusion or $q\bar{q}$ annihilation. During flavour excitation gluon fragmentation to a $b\bar{b}$ pair occurs in the initial state and results in one of the b quarks being scattered from the initial state to the final state by a gluon or light quark. The final category contains events where the $b\bar{b}$ pair are produced in the final state either within a parton shower or during the fragmentation process of a gluon or light quark.

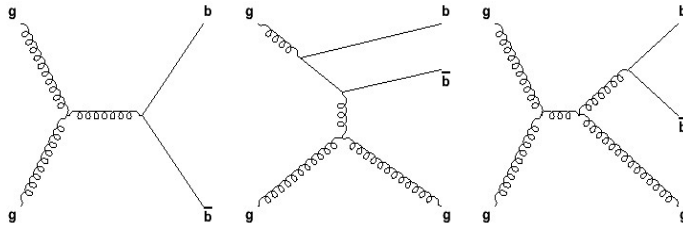


Figure 1: *Feynman diagrams for the various production classes. The diagram on the left shows flavour creation, the one in the centre shows flavour excitation and the right hand one shows gluon splitting*

Although events from the various categories cannot be fully separated, there are various kinematic characteristics which allow some distinction to be made as shown by

Rick Field (CDF/University of Florida) [4].

3 Data Samples

The data sample used contains events triggered by a 20 GeV jet trigger, the integrated luminosity of the dataset is $64.5 \pm 3.9 pb^{-1}$. In order to make comparisons to Leading Order predictions two Monte Carlo datasets are used: A Pythia [5] sample using CTEQ5l PDFs, simulating generic $2 \rightarrow 2$ processes with $pt_{min} > 18 GeV$; and a Herwig [6] sample with CTEQ5l PDFs also simulating generic $2 \rightarrow 2$ processes with $pt_{min} > 18 GeV$. In order to make a Next to Leading Order comparison a MC@NLO [7] $b\bar{b}$ sample is used. Jets are made using the jet clustering algorithm with a cone size of 0.7.

4 Jet Energy Corrections

Generic jet energy corrections are applied to account for effects such as variations in detector response over η or non linearities in the detector due to un-instrumented regions, as well as the effects of multiple interactions in the events [8]. The generic corrections were carried out for light jets, therefore, a correction is required for b flavour jets to account for missing energy due to semileptonic decays. We define this correction by comparing the energy of jets reconstructed using stable HEPG particles (hadronic jets), to those reconstructed using calorimeter information (calorimetric jets).

Using the Pythia sample, the hadronic jets are classified as b-jets if a b-hadron is found within a cone of 0.7 around the jet axis ($\Delta R(jet - B) < 0.7$)¹, these are then matched to the calorimetric jets within the central region, $|\eta| < 1.2$, by requiring $\Delta R(hadronic - calorimetric) < 0.2$. The ratio of hadronic jet E_t to calorimetric jet E_t is found to be 1.157 and is used as the b-jet correction. The systematic uncertainty for the correction is found by repeating the study using a Herwig sample; the difference between the Herwig and Pythia ratio is 1.3% and is used as an estimate for the systematic uncertainty.

5 Event Selection

Candidate events must pass the 20GeV jet trigger and are required to have two secondary vertex tagged jets, both tagged jets must lie within $|\eta| < 1.2$. One of the tagged jets is required to have corrected transverse energy (E_t^{cor}) greater than 30GeV; The other tagged jet is required to have E_t^{cor} greater than 20GeV.

¹ $\Delta R = \sqrt{\Delta\eta^2 + \Delta\phi^2}$

6 Acceptance

The acceptance is calculated for b-jets in the central region using Monte Carlo. We count the number of events where hadronic b-jets satisfy the selection criteria, N^{gen} , and the number of events where corrected calorimetric b-jets satisfy the selection criteria, N^{rec} ; the trigger efficiency is folded into the calculation by weighting each calorimetric event by the trigger efficiency for the lead jet. The acceptance is calculated using equation 1 to be 1.03 ± 0.02 .

$$A_{trig} = \frac{\sum^{N^{rec}} \epsilon_{trig}(lead\ jet)}{N^{gen}} \quad (1)$$

Changes to the jet energy corrections will change N^{rec} and are a source of systematic uncertainty. The systematic uncertainty for each level of corrections is shown in table 1, these are summed in quadrature to give a positive error of 18.2% and a negative error of 19.8%.

Correction	+ systematic	- systematic
Level 1	9.3%	10.8%
Level 2	0	0
Level 3	12.8%	13.7%
Level 4	0	0
Level 5	8.1%	8.5%
b correction	3.9%	4.0%

Table 1: *Systematic uncertainty on acceptance from each level of corrections*

To estimate the systematic uncertainty due to particle density functions (PDFs), the acceptance is calculated for samples with different PDF sets; a systematic uncertainty of 4.5% is assigned. The PDF systematic is combined in quadrature with the jet corrections systematic to give a total systematic uncertainty of +18.7% -20.3% on the acceptance.

To calculate the acceptance as a function of the leading jet's E_t^{cor} ², the azimuthal angle between the lead jet and second jet ($\Delta\phi$); and the dijet invariant mass; N^{rec} is binned in terms of the measured calorimetric jet values and N^{gen} is binned in terms of hadronic jet values, equation 1 is used to calculate the acceptance for each bin. Figure 2 shows the acceptance as function of the leading jet's E_t^{cor} , $\Delta\phi$ and the dijet invariant mass.

²The jets are arranged in decreasing E_t^{cor}

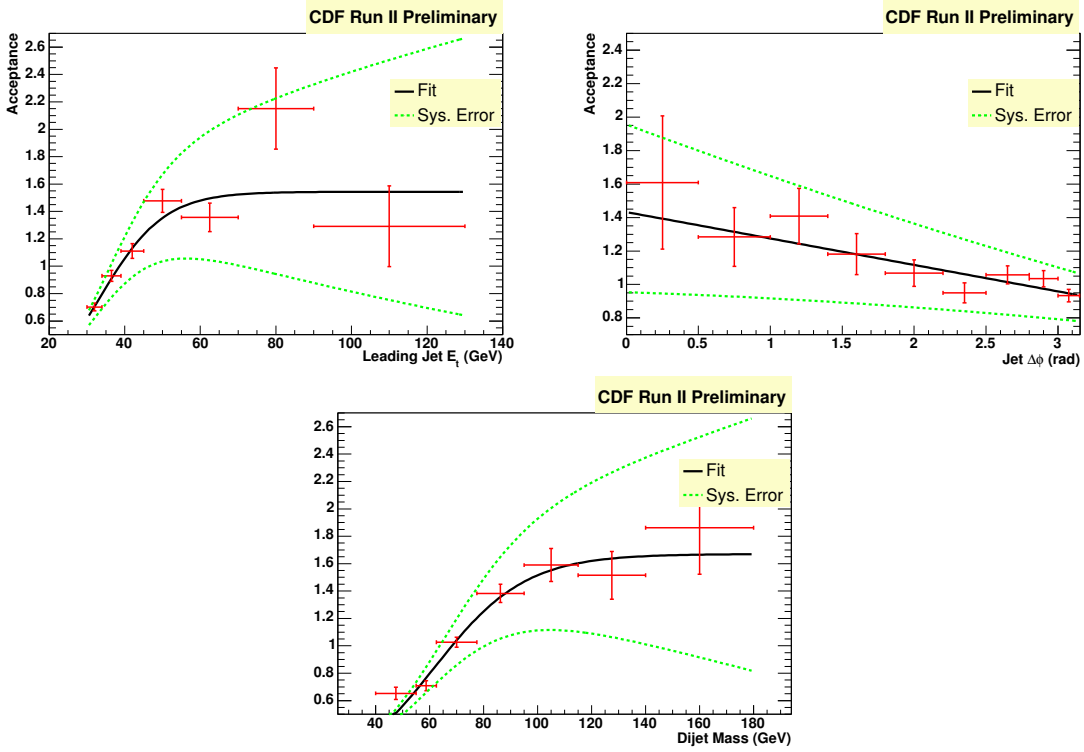


Figure 2: Event selection efficiency as a function of the leading jet's E_t^{cor} , $\Delta\phi$ between the lead jet and second jet and the dijet invariant mass of the leading jet and second jet.

7 Secondary Vertex Tagging Efficiency

High p_t electron samples are used to measure the tagging efficiency since the presence of a lepton enriches the b-quark content. Events passing an 8 GeV electron trigger are used; electron jets are selected by requiring jet $E_t > 15\text{ GeV}$ and $\Delta R(\text{electron} - \text{jet}) < 0.7$. To further enrich the sample with heavy flavour the event is required to have another jet that is secondary vertex tagged.

Using templates for b and non- b jets, the fractions of each in a data sample can be measured using a ROOT fitting function [9] called TFractionFitter [10]. Using the b fraction before and after applying the secondary vertex tag to the electron jets, the efficiency is defined as:

$$\epsilon_b = \frac{F_b^{tag} N^{tag}}{F_b^{ejet} N^{ejet}} \quad (2)$$

where N^{ejet} is the number of events in the sample and N^{tag} is the number of events with a tagged electron jet. To find the b flavour content of the sample (F_b^{ejet}) the spectrum for the electron's momentum relative to the jet axis is used; the secondary

vertex mass spectrum of the tagged electron jets is used to find the b flavour content of the events containing a tagged electron jet(F_b^{tag}).

We plot ϵ_b as a function of jet E_t in figure 3. A systematic uncertainty is assigned for the fit to the efficiency using the errors on the fit parameters. The efficiency measured is for semileptonic b decays, the efficiency for all decays is higher and a scale factor is introduced to account for this; half the difference between the scale factor and 1 is taken as the systematic uncertainty, an uncertainty of 7.7%. A 3.5% systematic uncertainty is applied for the uncertainty in the b fraction, calculated by measuring the b fraction of the sample using the secondary vertex mass of the second tagged jet in the event.

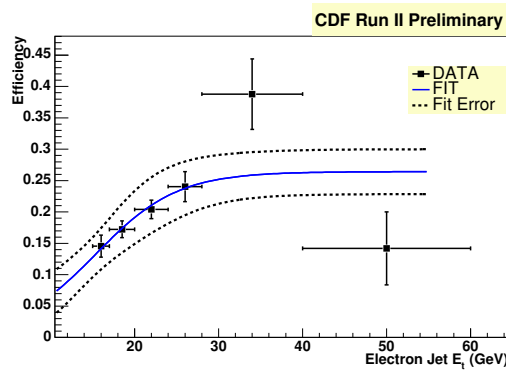


Figure 3: *SECVTX* tagging efficiency in data, together with the fit and the corresponding error.

8 Cross Section Calculation

The following formula is used to calculate the cross section:

$$\sigma_{b\bar{b}}(|\eta| < 1.2) = \frac{N^{ev} F_b^{ev}}{\epsilon_b^{lead} \epsilon_b^{other} A_{trig} \int L} \quad (3)$$

N^{ev} is the number of events in the sample after event selection and F_b^{ev} is the fraction of these events that contain b quarks. Since the two tagged jets will have different energies, their tagging efficiencies will be different, ϵ_b^{lead} is the tagging efficiency of the lead jets and ϵ_b^{other} is the tagging efficiency for the other tagged jet in the event. A_{trig} is the acceptance with trigger efficiency folded into it. $\int L$ is the integrated luminosity.

To find the b flavour content of the sample secondary vertex mass templates are derived from Monte Carlo, shown in figure 4, and used to fit the spectrum in data. Figure 5 shows the fit to the secondary vertex mass spectrum in data, the mass spectrum used is the combination of both tagged jets. The fit returns a b fraction of 0.83 ± 0.04 , the error accounts for the statistical uncertainties in the data and Monte Carlo spectra.

and is used as the statistical error for the cross section. A systematic uncertainty is applied by fitting the high and low E_t jets separately and taking the largest difference from the fit to the combined spectrum, giving an uncertainty of 3.0%.

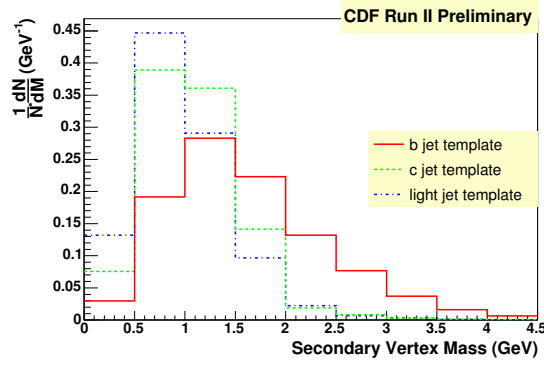


Figure 4: *Secondary vertex mass spectra used for fits to find purity of samples.*

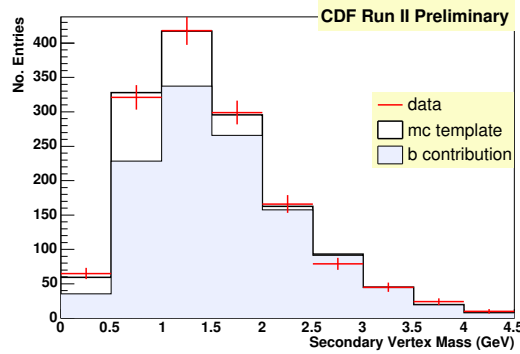


Figure 5: *Plots showing predicted histograms returned from $TFractionFitter$ together with the spectrum for the Data sample.*

The results for data, the Leading Order Pythia and Herwig predictions and the Next to Leading Order MC@NLO prediction are shown in table 2. Data agrees with the Pythia the prediction, however, the predicted cross section by both Herwig and MC@NLO are lower than Pythia. The systematic errors are summarised in table 3

The differential cross section as a function of the E_t^{cor} of the leading tagged jet and as a function of the invariant mass of the two tagged jets is shown in figures 6 and 7, respectively. They show agreement between Pythia and data, but both Herwig and MC@NLO are lower.

The differential cross section as a function of azimuthal angle, $\Delta\phi$, between the two jets is shown in figure 8. Data agrees with Pythia predictions, although there is

	Value
N_{events}	716
p^{events}	0.83 ± 0.04
ϵ_b^{lead}	0.31
ϵ_b^{other}	0.26
A_{trig}	1.03
$\int L$	$64.5 pb^{-1}$
$\sigma_{b\bar{b}}(\eta < 1.2)$	$34.5 \pm 1.8 nb$
Pythia(CTEQ 5l) σ	$38.7 \pm 0.6 nb$
Herwig (CTEQ 5l) σ	$21.5 \pm 0.7 nb$
MC@NLO σ	$28.5 \pm 0.6 nb$

Table 2: Results for the cross section calculation, all errors are statistical.

Systematic Uncertainty	$\sigma_{b\bar{b}}(nb)$
F_b	± 1.0
luminosity	± 2.1
ϵ_b	± 5.5
Acceptance	± 7.0
Final Value	$34.5 \pm 1.8 \pm 10.5$

Table 3: Systematic errors on the cross section and the final value with the associated statistical and systematic error

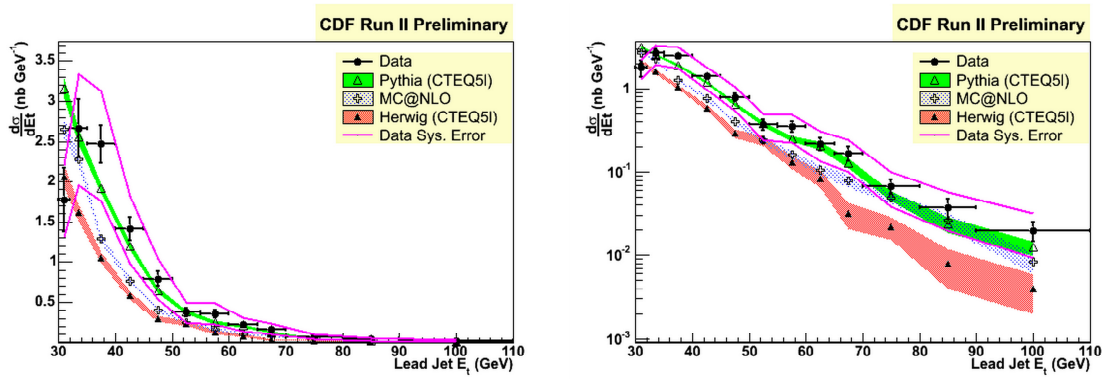


Figure 6: The differential cross section as a function of E_t^{cor} of the highest E_t tagged jet, shown on both linear(left) and log(right) scales.

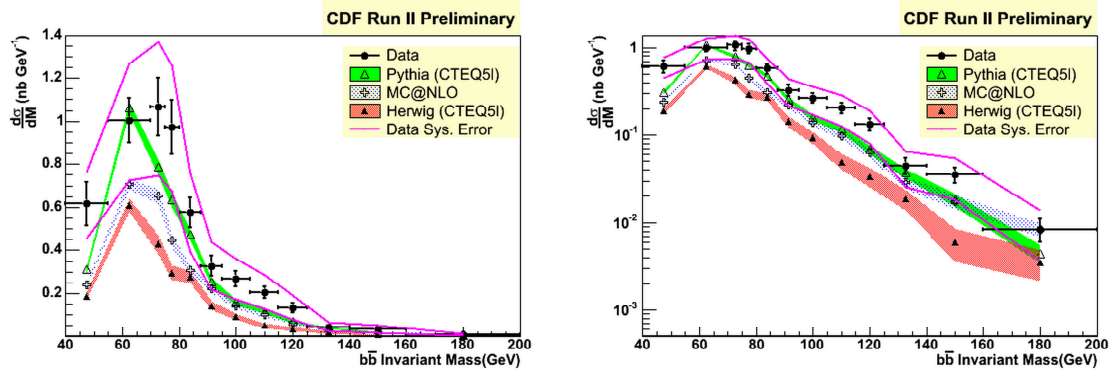


Figure 7: The differential cross section as a function of the invariant mass of the two tagged jets, shown on both linear(left) and log(right) scales.

some deviation at smaller opening angles. The difference between leading order and next to leading order predictions is highlighted in this plot; for both of the Leading Order Monte Carlos the differential cross section continues to fall as $\Delta\phi$ gets smaller, since the leading order process produces back-to-back b jets; However for MC@NLO the differential cross section starts to flatten out at small $\Delta\phi$ as a result of the flavour excitation and gluon splitting processes that are possible at Next to Leading Order.

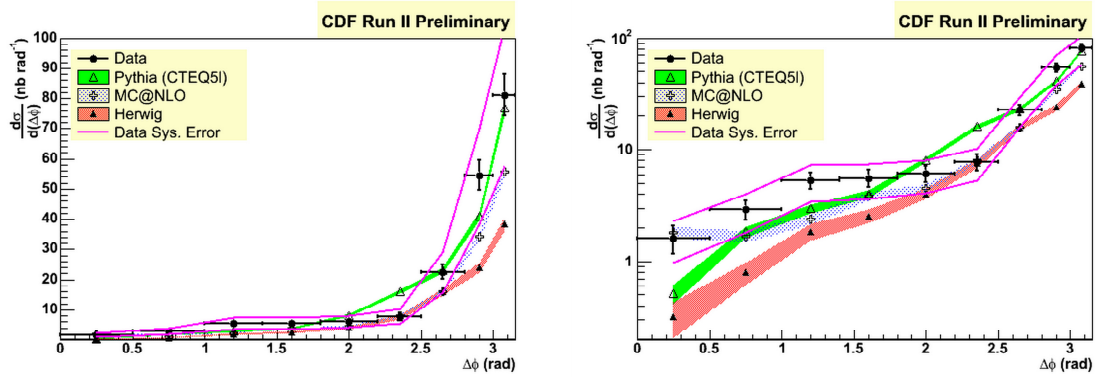


Figure 8: The differential cross section as a function of the azimuthal angle $\Delta\phi$ between the tagged jets, shown on both linear(left) and log(right) scales.

A generator called JIMMY [11], written by J. M. Butterworth, J. R. Forshaw and M. H. Seymour, is available for linking with Herwig. It generates multi-parton interactions

for Herwig, and thus provides a simulation of the underlying event.³ A small MC@NLO sample was generated with JIMMY used in conjunction with Herwig to see if this improved the MC@NLO jet predictions. The MC@NLO cross section calculated using this sample is $35.7 \pm 2.0 \text{ nb}$ which is in agreement with data and Pythia. The differential cross sections are shown in figure 9. There is good agreement with data, the differential cross section as a function of $\Delta\phi$ appears to agree better with this sample than with the Leading Order Pythia prediction.

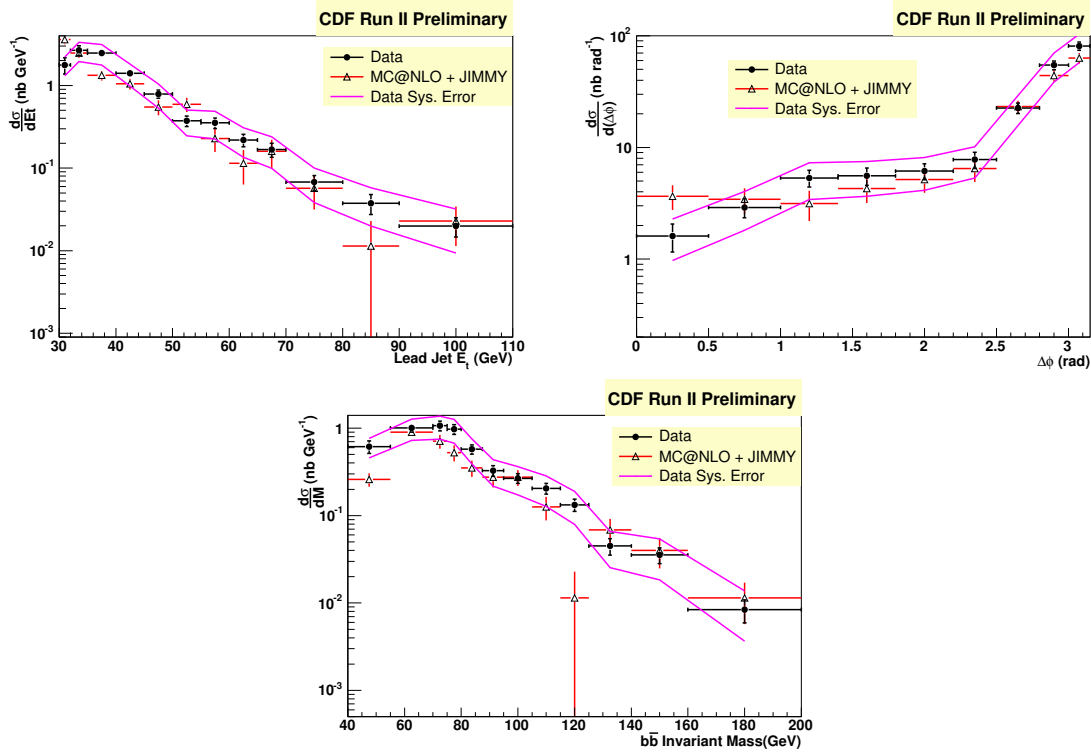


Figure 9: The differential cross section as a function of lead jet E_t , $\Delta\phi$ and invariant mass of the two jets for data and a MC@NLO prediction with JIMMY used in conjunction with Herwig.

9 Conclusions

We have measured the inclusive $b\bar{b}$ jet production cross section for events containing two SECVTX tagged jets within $|\eta| < 1.2$, where one of the jets has $E_t^{cor} > 30 \text{ GeV}$ and the other $E_t^{cor} > 20 \text{ GeV}$. We find $\sigma = 34.5 \pm 1.8 \pm 10.5 \text{ nb}$ and compare this to the value calculated using Pythia(CTEQ51) of $38.7 \pm 0.6 \text{ nb}$, Herwig(CTEQ51) of 21.5 ± 0.7

³The interactions generated are between the soft remnants after the hard scatter, multiple hard scatters are not generated.

and that calculated using MC@NLO of $28.5 \pm 0.6nb$. We have also calculated the differential cross section as a function of jet Et, the azimuthal angle between the jets and the invariant mass of the two jets. In all cases we find that Pythia models the data well and both Herwig and MC@NLO are lower than that observed in data.

The differential cross section as a function of azimuthal angle shows that the event selection picks out the leading order flavour creation processes however at small opening angles the effect of Next to Leading Order corrections is apparent; the measured cross section deviates from Pythia at these small opening angles.

MC@NLO is in better agreement with data, and Pythia, when JIMMY is used in conjunction with Herwig, which provides a better model for the underlying event; the differential cross section as function of $\Delta\phi$ shows particularly good agreement with data. The agreement between Leading Order and Next to Leading Order is expected since the event selection picks out the flavour creation process; calculations by S. Frixione et al. [12] also show that Next to Leading Order predictions are very similar to leading order when two b's are required within the event.

10 References

References

- [1] F. Abe et al., Measurement of the B Meson Differential Cross Section $d\sigma/dp_t$ in $p\bar{p}$ collisions at $\sqrt{s} = 1.8\text{TeV}$, Phys. Rev. Lett. 75 1451 (1995).
- [2] B. Abbott et al., The b Production Cross Section and Angular Correlations in $p\bar{p}$ collisions at $\sqrt{s} = 1.8\text{TeV}$, Phys. Lett. B487 264 (2000).
- [3] M. Cacciari and P. Nason, Is There a Significant Excess in Bottom Hadroproduction at the Tevatron?, Phys. Rev. Lett. 89 122003 (2002).
- [4] R. Field, The Sources of b-Quarks at the Tevatron and their Correlations, Phys. Rev. D65 094006 (2002).
- [5] T. Sjostrand et al., High-Energy-Physics Event Generation with PYTHIA 6.1, Comp. Phys. Comm. 135 238 (2001).
- [6] G. Corcella et al., HERWIG 6: an event generator for hadron emission reactions with interfering gluons (including supersymmetric processes), JHEP 01 010(2001).
- [7] S. Frixione et al., Matching NLO QCD computations and parton shower simulations, JHEP 06 029 (2002).
- [8] Jet Corrections Group at CDF,
<http://www-cdf.fnal.gov/physics/new/top/public/jets/cdfpublic.html>

- [9] ROOT TFractionFitter Page,
<http://root.cern.ch/htmldoc/TFractionFitter.html>
- [10] R. Barlow and C. Beeston, Fitting using finite Monte Carlo samples, *Comp. Phys. Comm.* 77 219-228 (1993).
- [11] JIMMY Generator - Multi-parton Interactions in HERWIG,
<http://jetweb.hep.ucl.ac.uk/JIMMY/index.html>
- [12] S. Frixione et al., Matching NLO QCD and parton showers in heavy flavour production, *JHEP*08 007 (2003)